Proceedings of the 8th International
IEEE Conference on Intelligent Transportation Systems
Vienna, Austria, September 13-16, 2005



# A High-Range-Resolution Microwave Radar System for Traffic Flow Rate Measurement

Yiguang Xuan, Huadong Meng, Xiqin Wang, Hao Zhang

*Abstract*—**The estimation of traffic flow parameters is a fundamental problem in Intelligent Traffic Systems. This paper presents a system based on a microwave radar with high range resolution and short sweep time to estimate the flow rate of traffic stream. Radar echoes are organized into sequential height images. The sequential height images contain all reflecting point information and thus give out detailed height distribution of echo intensity. By processing the height images with our vehicle detection and classification algorithms, passing vehicles can be automatically detected and simultaneously classified into eight types.**

## I. Introduction

THE measurement of traffic flow parameters is of great importance to the development of traffic flow models and traffic control systems. Flow rate, which is defined as the number of passing vehicles at a point in unit time, is important in describing and understanding the properties of traffic flow. However, vehicles are not identical, and different vehicles have different influence on traffic flow. One way to deal with this problem is to convert daily flow rate into certain equivalent flow rate by weighting different vehicle types with different coefficients. Since we do not have the coefficients, we will estimate the flow rates of different types of vehicle. For this purpose, we need to estimate traffic flow rate and vehicle types simultaneously.

Many solutions have been introduced in the estimation of these two parameters. Inductive loop [1], [2] is the cheapest choice, but it has the disadvantage that they are difficult to install and are liable to damage by tarmac subsidence. Vision-based sensor (monocular [3], [4], [5], or binocular [6]) can provide the richest information of traffic flow, and has been most frequently adopted. But the algorithms for vision-based vehicle detection and classification are much complicated when the weather or light condition is not ideal. Laser sensor [7], [8] can provide detailed depiction of the vehicle, due to its narrow beam width, but it is vulnerable to rain and mist. Microwave radar is not sensitive to light, and thus robust in all kinds of weather conditions. Among the two types of microwave radars, the FMCW (frequency modulated continuous wave) microwave radar sensors [9] do not have enough distance resolution for detailed description of the passing vehicles, while pulse microwave radar behaves well in vehicle detection and classification in [10]. There are also some existing automatic vehicle detection and classification system [11], which usually combines several sensors together to get a better performance.

In our experiments, a pulse microwave radar featuring high range resolution and short sweep time was used. At a certain distance that is controlled linearly by an external input signal, the radar can judge the existence of objects through the echo intensity. When the radar is given a fast-varying control signal, the radar may sweep fast over a series of distances with high distance precision, due to its high range resolution and short sweep time. In our experiments, the radar was put above a lane, and given a continually fast-varying control signal, and then we might get the radar-to-objects distance information precisely and continually. If a vehicle passed below the radar, we would get the height profile of the vehicle. The echo intensities are organized into sequential height images in the format of gray-scale images, on which our detection and classification is based.

The remainder of this paper is organized as follows. Section II is a brief introduction to the system we developed for the experiments and the process of the experiments. We will analyze the data and introduce the algorithms for vehicle detection and classification in Section III, and conclude in Section IV.

## II. Methodology

### A. Description of the sensor system

The main components of the radar system are shown in Fig. 1. The pulse radar has three signal channels, one input control channel and two output channels (inphase and quadrature). The input channel was connected to the D/A converting channel of a DAQ (data acquisition) card, whereas the output channels were connected to two of the A/D converting channels of the card. The DAQ card was located in the PCI slot of a computer. Through programming, the computer sent out control signals to the input control channel of the radar through the D/A converting channel. At the same time, the computer recorded the output signals through the A/D converting channels onto the hard disk.

Manuscript received March 4, 2005.

Yiguang Xuan is with the Tsinghua University, Beijing 100084, P.R.China (e-mail: xyg@mails.tsinghua.edu.cn).

Huadong Meng is with the Tsinghua University, Beijing 100084, P.R.China (e-mail:menghd@tsinghua.edu.cn).

Xiqin Wang is with the Tsinghua University, Beijing 100084, P.R.China (phone: 86-10-62781378; fax: 86-10-62770317; e-mail: wangxq_ee@tsinghua.edu.cn).

Hao Zhang is with the Tsinghua University, Beijing 100084, P.R.China (email:haozhang@tsinghua.edu.cn).

0-7803-9215-9/05/$20.00 ©2005 IEEE.

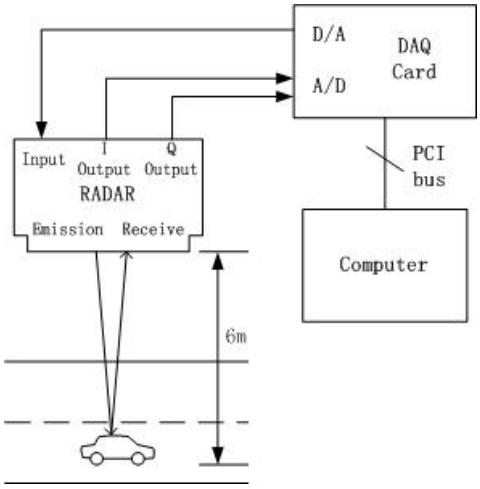

Fig. 1. Main components of the radar system.

### B. High-range-resolution (HRR) microwave radar

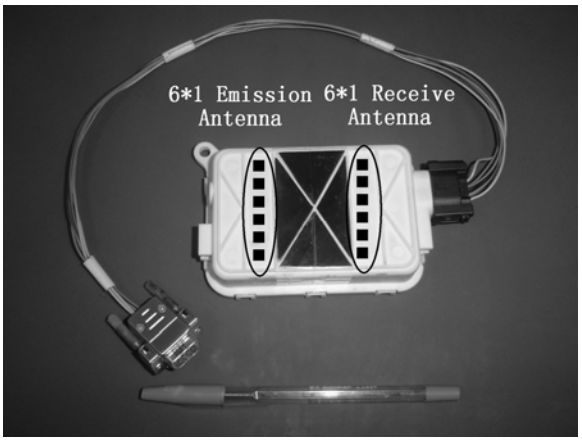

Fig. 2. HRR microwave radar, in contrast with a ball pen.

The analog HRR microwave radar sensor [12] produced by "AMP MA/COM" is a pulse radar featuring ultra-short pulses, which ensure a very high resolution and accuracy of about 6cm. The sensor is a small lightweight design, depicted in Fig. 2. The sensor antennas are separated 6×1 patch arrays for the transmission and receive side.

Some technical data of the radar are shown in Table I.

TABLE I
SOME TECHNICAL DATA OF THE HRR MICROWAVE RADAR

| PARAMETER | MIN. | TYP. | MAX. | UNIT |
|---|---|---|---|---|
| Carrier Frequency | | 24.125 | | GHz |
| Pulse width | 300 | 350 | 400 | ps |
| Pulse Repetition Interval | | 250 | | ns |
| Range | 0.15 | | 20 | m |
| Sweep Time | 1 | 20 | | ms |
| Average Power | -22 | -20 | -19 | dBm |
| Peak Power | 4 | 5 | 6 | dBm |

The block diagram of the microwave radar is shown in Fig. 3.

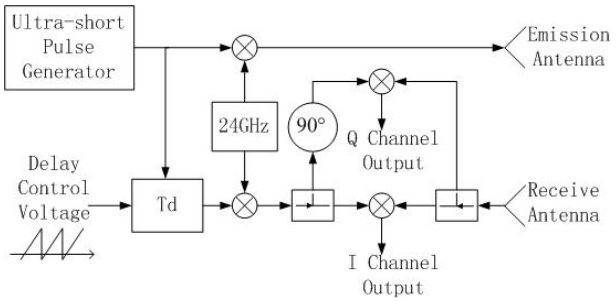

Fig. 3. Block diagram of the HRR pulse microwave radar.

Ultra-short pulses of about 350ps are generated, and transmitted after modulation. The signal is then received after some delay, which contains the distance information. Only if this delay coincides with the delay controlled linearly by the external delay control voltage, will there be output in the inphase (I) and quadrature (Q) channels. And during each scanning, we will know the status a certain distance away, which is specified by the delay control voltage. Therefore, if given a continually fast-varying delay control voltage, we may get the radar-to-objects distance information precisely and continually.

The beam width along the traffic flow is narrow (13 degrees), which enable us to measure objects that are only right below the radar. The beam width transversal to the traffic flow is wide, and we can detect the vehicle even when it presents partially in lane. All these will help us count correctly in multilane conditions, and will be introduced in Section III.

### C. Process of the experiment

The radar was fixed above a lane on a highway in Beijing, with a perpendicular distance of about 6 meters to the middle of the lane (Fig. 1). While the radar was working, there was a digital video recording the passing vehicles for reviewing.

The sampling frequency of the A/D channel on the DAQ card was set to be about 33KHz per channel (100KHz for three channels). Input control signal of the radar was programmed to be a 100Hz serrate wave. So if a 5-meter-long vehicle passes right below the radar with a speed of 50kmh, it will be swept 36 times. The input control voltage was between 0.9V and 1.9V, which corresponded to a distance between 1.1m and 6.9m to the radar. This means the radar was sweeping a range of about five meters above the ground.

## III. ANALYSIS OF THE EXPERIMENT DATA

### A. Preprocessing of data

The data were read from the hard disk, and divided into three channels of signals – the input control signal $SC$, the I channel output $SI$, and the Q channel output $SQ$. Through these vectors, we got the output signal, which is also the echo intensity $S_i = \sqrt{SI_i^2 + SQ_i^2}$, where the subscript *i* denotes index of sampling series.

The echo intensity $S$ (a vector) then was reorganized into sequential height images, in the format of a large gray-scale image (a two-dimensional array), with one dimension corresponded to sweep number or time, and the other dimension corresponded to the heights of the reflecting objects above the ground. The gray-scale values of the pixels in the image denote the echo intensities. In order to reduce the operation complexity, we broke the whole image into a series of smaller frames of image. All frames of image have the length of 150 sweeps, with a step of 10 sweeps between every two frames. (One of the frames is shown in Fig. 4.)

For the convenience of reader, the values of our height images have been inverted, with small gray-scale values (black) denote large echo intensities.

### B. *Vehicle detection*

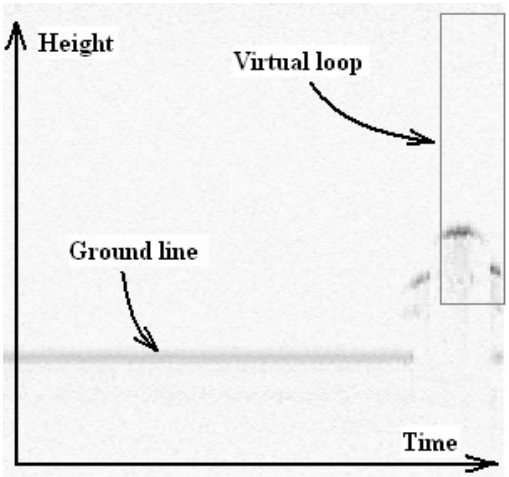


Fig. 4. Vehicle detection. The figure is the gray-scale image frame of a passenger car. The gray-scale value denotes the intensity of echo. The virtual loop has been indicated in the figure. The black line parallel to the time-axis denotes the ground echo.

First, we estimate the existence of reflecting objects. We assume that the I (inphase) and Q (quadrature) channel noise outputs are subject to normal distribution independently and identically

$$SI_i, SQ_i \sim \mathrm{N}(0, \sigma^2) \quad i.i.d. \tag{1}$$

Then the noise echo intensity $S_i = \sqrt{SI_i^{\,2} + SQ_i^{\,2}}$ is subject to Rayleigh distribution. Given an error probability $P_\alpha$, the threshold $th$ of the echo intensity is determined by

$$\int_{th}^{\infty} \frac{x}{\sigma^2} e^{-\frac{x^2}{2\sigma^2}} dx = P_\alpha \tag{2}$$

A virtual loop (Fig. 4) is placed in every frame of image. In our experiments, the loop's lower and upper boundaries correspond to the height of 0.5m and 3.5m above the ground, and the length of the loop is 20 sweeps. The existence of the passing vehicle is based on the number of reflecting points at certain height in the virtual loop. If a vehicle passes below the radar, there will be a serial of reflecting objects at certain height. In our experiments, we assume that if there are more than three reflecting objects at certain height, a vehicle is present below the radar.

The results of vehicle detection are shown in Table II. In our detection results, all the vehicles in the below-the-radar lane (Column 2) are successfully detected, with no false alarm (Column 4), except for a few missing vehicles (Column 3). Some vehicles out of the below-the-radar lane (Column 5) have also been detected due to their large reflecting size. And Column 6 is the total number of vehicles detected.

TABLE II
VEHICLE DETECTION RESULTS

| FILE NUM | VEHICLES IN-LANE | VEHICLES MISSING | FALSE ALARM | OUT-LANE DETECTED | TOTALLY DETECTED |
|---|---|---|---|---|---|
| 1 | 122 | 2 | 0 | 13 | 133 |
| 2 | 113 | 1 | 0 | 19 | 131 |
| 3 | 182 | 2 | 0 | 23 | 203 |

### C. *Vehicle classification*

First, we define a vehicle type list, as in Table III.

TABLE III
VEHICLE TYPES

| TYPE SYMBOL | TYPE NAME |
|---|---|
| T12 | Passenger car (hatchback) |
| T13 | Passenger car (saloon) |
| T14 | Jeep |
| T21 | Minibus (shorter) |
| T22 | Minibus (taller) |
| T31 | Bus |
| T41 | Lorry |
| T42 | Van |

The frames containing vehicles are auto-detected, and extracted. Actual vehicle types are then identified by reviewing the simultaneously recorded digital video. In Fig. 5, we notice that the maximal heights of different types of vehicles are distributed without much overlapping, so we use maximal height of vehicle to do a preliminary classification. The results of the preliminary classification are shown in Table IV.

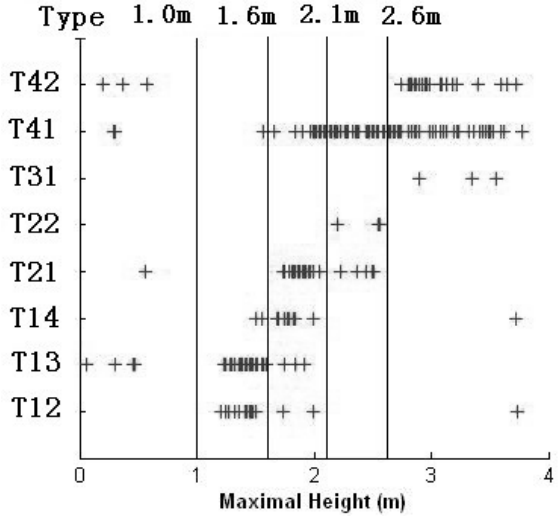


Fig. 5. Preliminary classification result. X-axis is maximal height of the vehicle. Y-axis corresponds to different vehicle types.

TABLE IV
PRELIMINARY CLASSIFICATION RESULT

| CATEGORY NUMBER | MAXIMAL HEIGHT | PRELIMINARY CLASSIFICATION RESULT |
|---|---|---|
| 0 | 0m – 1.0m | Error (due to weak echo, etc.) |
| 1 | 1.0m – 1.6m | T12, T13 |
| 2 | 1.6m – 2.1m | T14, T21, T41 |
| 3 | 2.1m – 2.6m | T22, T41 |
| 4 | >2.6m | T31, T41, T42 |

After preliminary classification, we need to distinguish different vehicle types in the same category. This is done through template matching. We assign every type with a template, denoting the standard height profile of the specific type of vehicle. If we take the template height profile, which is in the format of a vector with length $N$, as a vector in the $N$-dimensional vector space, the distance between the vectors can be taken as a metric of the similarity of the corresponding vehicle height profiles.

The process of the template matching is described below. A series of normal orthogonal basis is obtained after doing Gram-Schmidt orthogonalization on templates in the same category. For example, in a certain category, if there are $M$ templates corresponding to the $M$ types in the category respectively

$$\begin{aligned} \boldsymbol{h}_1 &= (h_{11}\ h_{12}\ \cdots\ h_{1N})^T \\ \boldsymbol{h}_2 &= (h_{21}\ h_{22}\ \cdots\ h_{2N})^T \\ &\vdots \\ \boldsymbol{h}_M &= (h_{M1}\ h_{M2}\ \cdots\ h_{MN})^T . \end{aligned} \tag{3}$$

Gram-Schmidt orthogonalization on $[\boldsymbol{h}_1\ \boldsymbol{h}_2\ \cdots\ \boldsymbol{h}_M]$ results in $M'$ normal orthogonal bases $[\boldsymbol{\alpha}_1\ \boldsymbol{\alpha}_2\ \cdots\ \boldsymbol{\alpha}_{M'}]$ and a $M' \times M$ coefficient matrix ($M' \le M$)

$$[\boldsymbol{h}_1\ \boldsymbol{h}_2\ \cdots\ \boldsymbol{h}_M] = [\boldsymbol{\alpha}_1\ \boldsymbol{\alpha}_2\ \cdots\ \boldsymbol{\alpha}_{M'}] \begin{bmatrix} c_1^{(1)} & \cdots & c_M^{(1)} \\ \vdots & \ddots & \vdots \\ c_1^{(M')} & \cdots & c_M^{(M')} \end{bmatrix}. \tag{4}$$

We normalize the length of the target vehicle height profile to $N$, through linear interpolation and sampling. Then we project the $N$-dimensional vector $\boldsymbol{h}_t = (h_{t1}\ h_{t2}\ \cdots\ h_{tN})^T$ onto the normal orthogonal bases $[\boldsymbol{\alpha}_1\ \boldsymbol{\alpha}_2\ \cdots\ \boldsymbol{\alpha}_{M'}]$, to get $M'$ projecting coefficients $[c_t^{(1)}\ c_t^{(2)}\ \cdots\ c_t^{(M')}]^T$. We calculate the distances between the target and the $M$ templates

$$d_{it} = \sqrt{(c_i^{(1)} - c_t^{(1)})^2 + (c_i^{(2)} - c_t^{(2)})^2 + \cdots + (c_i^{(M')} - c_t^{(M')})^2}, \tag{5}$$
$$i = 1 \cdots M.$$

And we take the type of the $i$th template, which has the smallest distance $d_{it}$, as the type of the target vehicle.

The results of the template matching in Category 1, 2, 3, and 4 are shown in Fig. 6, Fig. 7, Fig. 8, and Fig. 9 respectively. In Fig. 6 and 8, $c^{(1)}$ and $c^{(2)}$ are the two projecting coefficients on the normal orthogonal bases of the corresponding category. In Fig. 7 and 9, $c^{(1)}$, $c^{(2)}$, and $c^{(3)}$ are the three projecting coefficients on the normal orthogonal bases of the corresponding category.

The vehicle classification accuracies of the four categories are 85% (130/153), 82% (80/97), 88% (46/53), and 82% (73/89) respectively, with an average classification accuracy of 84% (329/392).

Now that we have classified the passing vehicles into the eight types in Table IV, we can obtain their corresponding flow rate.

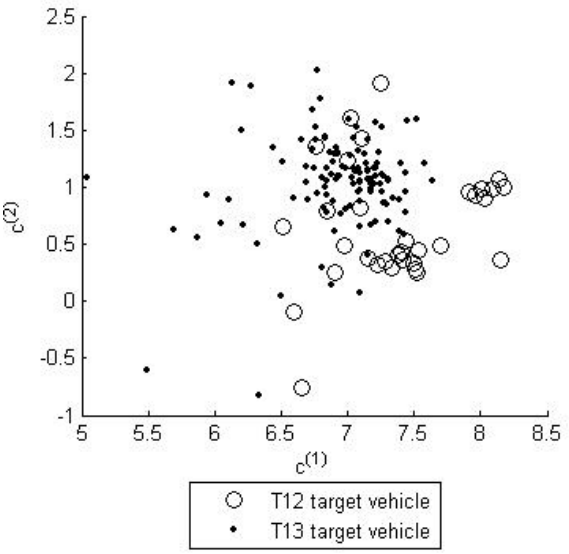


Fig. 6. Template matching result of Category 1 (85%). $c^{(1)}$ and $c^{(2)}$ are projecting coefficients onto the normal orthogonal bases of Category 1 with $M = M' = 2, N = 40$. The numbers of the T12 and T13 target vehicles are 33 and 120 respectively.

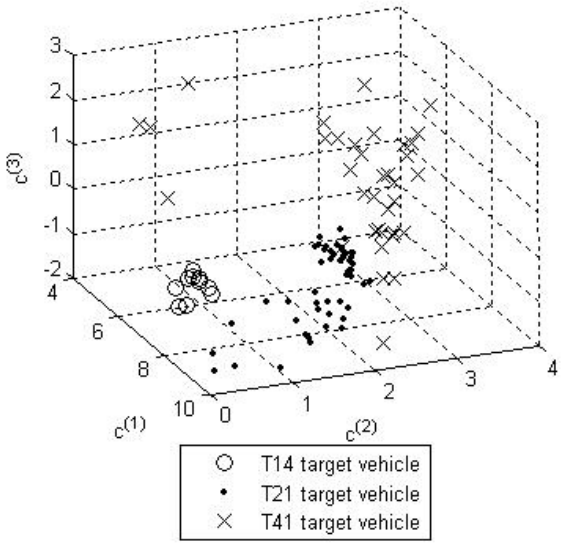


Fig. 7. Template matching result of Category 2 (82%). $c^{(1)}$, $c^{(2)}$, and $c^{(3)}$ are projecting coefficients onto the normal orthogonal bases of Category 2 with $M = M' = 3, N = 40$. The numbers of the T14, T21 and T41 target vehicles are 10, 51 and 36 respectively.

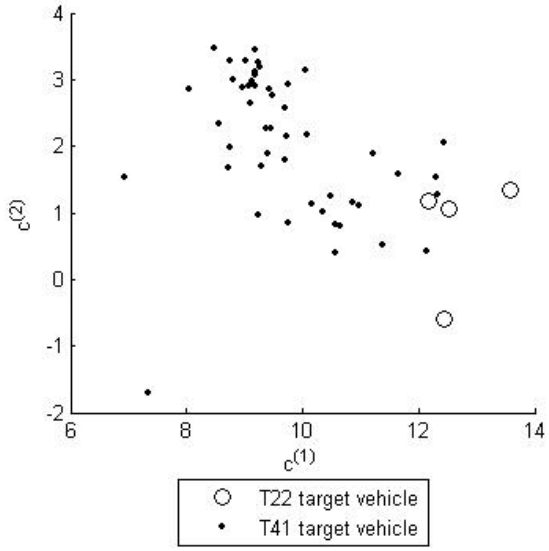


Fig. 8. Template matching result of Category 3 (88%). $c^{(1)}$ and $c^{(2)}$ are projecting coefficients onto the normal orthogonal bases of Category 3 with $M = M' = 2, N = 40$ . The numbers of the T22 and T41 target vehicles are 4 and 49 respectively.

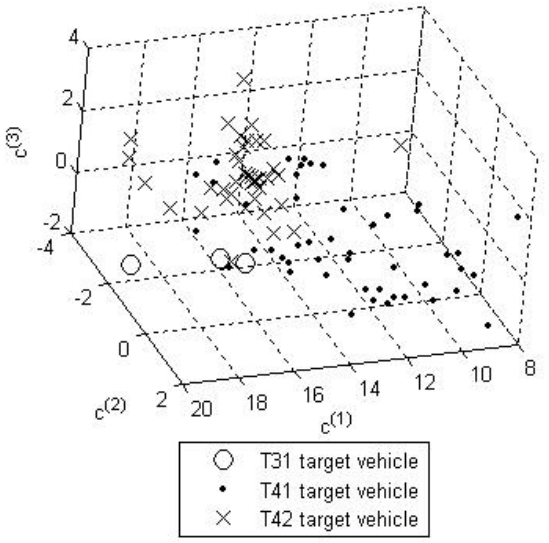


Fig. 9. Template matching result of Category 4 (82%). $c^{(1)}$, $c^{(2)}$, and $c^{(3)}$ are projecting coefficients onto the normal orthogonal bases of Category 4 with $M = M' = 3, N = 40$ . The numbers of the T31, T41 and T42 target vehicles are 3, 47 and 39 respectively.

### *D. Extra information that may improve performance*

Our experiment data also provide some extra information that we did not use in our algorithms, but we think the extra information is interesting and may improve the performance of the present system when properly used.

*1) The ground echo*

The ground echo intensity varies with the area of the ground exposed to the radar, which can approximately tell the lateral position of the vehicle, for example, in the middle of the lane (Fig. 10a), with some deflection (Fig. 10b), or already on the lane line (Fig. 10c). Making use of the ground echo intensity, the lateral position of the vehicle may help to improve detection in single lane or multilane conditions.

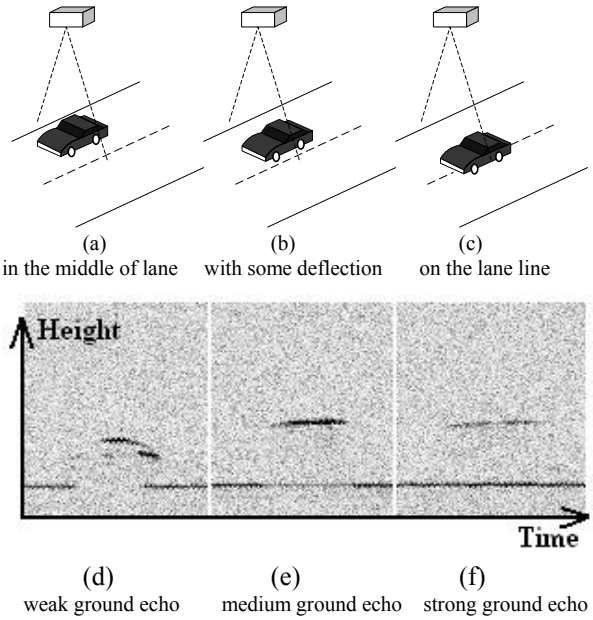


(a) in the middle of lane (b) with some deflection (c) on the lane line

(d) weak ground echo (e) medium ground echo (f) strong ground echo

Fig. 10. Variation of ground echo. (a), (b), (c) is the sketch map of the lateral position of the vehicle in lane. (d), (e), (f) is the gray-scale image when the vehicle is right below the radar in the situation of (a), (b), (c) respectively. (In the gray-scale image, the gray-scale value denotes echo intensity.)

*2) Multiply reflecting objects*

The gray-scale image can provide the richest height information about the vehicle, not just height profile (Fig. 11b), but also sequential height images (Fig. 11a). This may help us better know the vehicle. For example in Fig. 11, we notice that there are two black lines at the rear body of the truck. The upper thin line is the edge of the loading section, whereas the lower bolder line indicates that the loading section is empty, and is wider than the edge. The feature can also help us in the classification of vehicles.

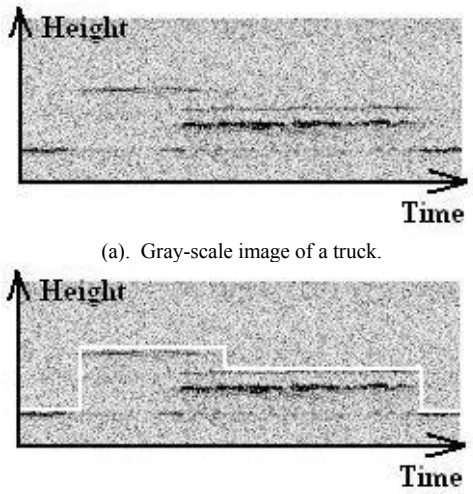


(a). Gray-scale image of a truck.

(b). The white line denotes the height profile of (a).

Fig. 11. Multiple reflecting objects.

## IV. CONCLUSION

A system based on HRR microwave radar sensor has been proposed to estimate traffic flow rate and the flow rate of certain types of vehicle. We organize the echo intensities into sequential height images in the format of a two-dimensional gray-scale image, on which our analysis is based. The sequential height images are then broken down into a series of frames of image. We calculate the threshold for reflecting object detection at a given error probability. Then by placing a virtual loop in every frame to count the number of reflecting objects in the loop, we can automatically detect the passing vehicles and estimate the flow rate. The vehicle detection result shows a zero false alarm rate, and a 1% missing rate. The frames of image that contain the detected vehicle are then extracted and the vehicles are preliminarily classified into four categories based on maximal height of the vehicles. Then a more detailed classification with eight types is achieved through template matching, with the average classification accuracy of 84%, and so the corresponding flow rate of every type of vehicle can be obtained. We have also noticed some extra information, such as ground echo and multiple reflecting objects, which might help to improve the performance of the present system.

The advantages of the present system include high range resolution, short sweep time, ability to detect multiple reflecting objects, wide transversal detection range, robust in all kinds of weather and light conditions, as well as light weight and small size. Still, there are also some problems. First, we do not provide any information along the traffic flow, such as the speed and length of the vehicle. This leads to some problems in classifying vehicles that are only different in length. Possible solutions include using a Doppler radar, or placing another radar identical to the one in this paper a distance away along the traffic flow, to get the speed information. Second, the radar system is restricted to some special locations, for example, the underside of a bridge, or a gantry, which is above a lane. Measurements cannot be carried out without proper locations. So a new system that can work at any location might be more attractive. Third, the classification algorithm is still not satisfactory. A more scientific vehicle type definition and a more detailed vehicle template library will both be helpful. And the identification of lorries, which may carry various loads, is worthy of some attention.

## ACKNOWLEDGMENT

The authors thank Prof. H. Rohling of Technische Universität Hamburg-Harburg for providing the HRR microwave radar and his kindly support to this work.

## REFERENCES

[1] J. Gajda, R. Sroka, M. Stencel, A. Wajda, and T. Zeglen, "A vehicle classification based on inductive loop detectors," Proceedings of the 18th IEEE Conference IMTC 2001, vol. 1, pp. 460-464, May 2001.

[2] R. Sroka, "Data fusion methods based on fuzzy measures in vehicle classification process", Instrumentation and Measurement Technology Conference, 2004. IMTC 04. Proceedings of the 21st IEEE, Vol. 3, May 2004, pp. 2234-2239.

[3] A. H. S. Lai, G. S. K. Fung, and N. H. C. Yung, "Vehicle type classification from visual-based dimension estimation," in Proceedings of IEEE Intelligent Transportation Systems, pp. 201-206, Aug. 2001.

[4] S. Gupte, O. Masoud, R. F. K. Martin, N. P. Papanikolopoulos, "Detection and classification of vehicles," in IEEE Transaction on Intelligent Transportation Systems, vol. 3, No. 1, pp. 37-47, Mar. 2002.

[5] Chunrui Zhang, and M.Y. Siyal, "A new segmentation technique for classification of moving vehicles", in Vehicular Technology Conference Proceedings, 2000. VTC 2000-Spring Tokyo. 2000 IEEE 51st, Vol. 1, May 2000, pp.323-326.

[6] M. J. J. Burden, and M. G. H. Bell, "Vehicle classification using stereo vision," in Image Processing and Its Applications, Sixth International Conference on, vol. 2, pp. 881-885, Jul. 1997.

[7] H. M. Abdelbaki, K. Hussain, and E. Gelenbe, "A laser intensity image based automatic vehicle classification system," in IEEE Proceedings on Intelligent Transportation Systems, pp. 460-465, Aug. 2001.

[8] William C. Schwartz, "Laser vehicle detector/classifier", in Proceedings of SPIE, Vol. 2344, 1995, pp. 81 -87.

[9] H. Roe, and G. Hobson, "Improved discrimination of microwave vehicle profiles," Microwave Symposium Digest, IEEE MTT-S International, vol. 2, pp. 717-720, June 1992.

[10] I. R. Urazghildiiev, R. Ragnarsson, K. Wallin, A. Rydberg, P. Ridderstrom, and E. Ojefors, "A vehicle classification system based on microwave radar measurement of height profiles," in RADAR 2002, pp. 409-413, Oct. 2002.

[11] S. Tropartz, E. Horber, and K. Gruner, "Experiences and results from vehicle classification using infrared overhead laser sensors at toll plazas in New York City", in Intelligent Transportation Systems, 1999. Proceedings. 1999 IEEE/IEEJ/JSAI International Conference on, Oct. 1999, pp. 686-691.

[12] D. Oprisan, and H. Rohling, "Analog high range resolution radar sensor, reference book", Technische Universität Hamburg-Harburg, June 2002.